ELSEVIER

Radiation damage tolerant nanomaterials

I.J. Beyerlein[1], A. Caro[1], M.J. Demkowicz[2], N.A. Mara[1], A. Misra[1,*] and B.P. Uberuaga[1]

[1] Los Alamos National Laboratory, Los Alamos, NM 87545, United States
[2] Massachusetts Institute of Technology, Cambridge, MA, United States

Designing a material from the atomic level to achieve a tailored response in extreme conditions is a grand challenge in materials research. Nanostructured metals and composites provide a path to this goal because they contain interfaces that attract, absorb and annihilate point and line defects. These interfaces recover and control defects produced in materials subjected to extremes of displacement damage, impurity implantation, stress and temperature. Controlling radiation-induced-defects via interfaces is shown to be the key factor in reducing the damage and imparting stability in certain nanomaterials under conditions where bulk materials exhibit void swelling and/or embrittlement. We review the recovery of radiation-induced point defects at free surfaces and grain boundaries and stabilization of helium bubbles at interphase boundaries and present an approach for processing bulk nanocomposites containing interfaces that are stable under irradiation.

Introduction

Materials under extreme environments have received significant attention recently in the context of next-generation energy, defense and transportation technologies. These applications require materials to perform at ''extremes'' of stress, temperature, irradiation dose, and corrosive environments [1]. The next-generation of nuclear power reactors require structural materials capable of withstanding elevated temperatures and radiation fluxes in highly corrosive environments for long periods of time without failure [1–3]. In land or air vehicles, lightweight, high-strength structural materials are needed to increase fuel efficiency and reduce exhaust gas emissions [1].

These increased demands of future technologies cannot be met by incremental improvements to conventional materials. New concepts in materials design are needed to manufacture materials that resist damage at irradiation and mechanical extremes [4]. It has long been known that surfaces, grain boundaries and interphase boundaries are sinks for radiation-induced point defects and traps for helium (produced as a transmutation product under neutron irradiation) [5–10]. There have been several recent studies in ferritic alloys containing dispersed nanoscale oxide particles where the oxide/ferrite interfaces are defect sinks and helium traps [11–20]. However, the detailed mechanisms at the level of the atomic structure of an interface that enable a nanocomposite to be stable under high irradiation flux or high concentration of helium are only just beginning to be clarified through studies on model systems where ion irradiation or implantation experiments are closely integrated with atomistic modeling [21–24]. Likewise, methods to process bulk nanocomposites, where the key is not just to refine the microstructure but also to produce interfaces that are stable at extreme conditions, are still under development [25].

This article presents an overview of recent developments in the understanding of defect recovery mechanisms in designed nanocomposites and an approach to process such materials in bulk form. The focus is on surface and interface phenomena in the context of model systems based on face-centered-cubic (fcc) or body-centered-cubic (bcc) metals. Such materials are ideal platforms for integrating theory with experiment and gaining mechanistic insights that provide the foundation for designing radiation-tolerant nanomaterials more generally.

*Corresponding author:. Misra, A. (amisra@lanl.gov)

1369-7021/06/$ - see front matter http://dx.doi.org/10.1016/j.mattod.2013.10.019

First, we present the case of a nanoporous single-phase metal. Since free surfaces are perfect defect sinks, this study provides an insight into the optimal length-scale (spacing between surface sinks) to maximize defect recovery. The first study suggests that enhanced defect recovery may be expected in single-phase nanostructured materials when the spacing between grain boundary sinks (i.e., grain size) is on the order of several tens of nanometers. However, it does not provide any insight into the mechanism via which vacancies and interstitials are annihilated at boundary sinks given the large difference in the migration energies of these two point defects. This mechanistic insight is captured in the second example of defect annealing at a grain boundary via an interstitial emission mechanism that enables rapid recombination of vacancies and interstitials despite the large difference in their mobilities. While the recombination of vacancies and interstitials is an important aspect of controlling void swelling in irradiated materials, an equally important challenge is managing helium that is produced as a transmutation product. Helium cannot be easily removed and hence, must be 'managed' by storing it in a stable form where it does not grow into an unstable void. The strategy to effectively store helium at interfaces is elucidated in our third example using an interphase boundary, where the atomic structure of the interface provides a dense array of sites for stable helium storage. The above effects were demonstrated in small-scale materials, typically in the form of thin films. In order for these concepts to be exploited in materials for nuclear power reactors, nanomaterials containing such interfaces must be processed in bulk form. An approach using accumulative roll bonding (ARB) to process bulk, radiation-resistant and thermally stable nanocomposites is presented in the fourth example. Deformation to large plastic strains during ARB leads to the formation of crystallographically stable interfaces and texture after a critical strain level. These crystallographically stable interfaces are also good point defect sinks and helium traps and stable under high dose irradiation, similar to the epitaxial interfaces studied in model thin film systems.

Defect recovery at surfaces in nanoporous metals

The key to perfect radiation endurance is complete recombination of all radiation-induced vacancies and interstitials. Since surfaces are perfect defect sinks, nanoporous materials, due to their high surface-to-volume ratio, have the potential to become a new class of extremely radiation tolerant materials. Furthermore, the nanoscale, dislocation-free ligaments may provide unusually high yield strengths.

In the case of nuclear fuels, which exhibit a natural foam-forming tendency due to fission gas accumulation, advanced fuels may be designed with a porous structure to accommodate the gas [26,27]. However a basic understanding of foam response in a radiation environment has so far been missing.

Nanoporous materials may also be relevant to the design of radiation-resistant spacecraft [28]. Knowledge of the radiation response of nanoporous materials also has applications in astrophysical sciences. Porous materials are ubiquitous in the universe and the weathering of porous surfaces plays an important role in the evolution of planetary and interstellar materials [29–31]. The sputtering of porous solids in particular can influence atmosphere formation, surface reflectivity, and the production of the ambient gas around materials in space.

The synthesis of nanoscale foams of noble metals is simple. Nanoporous Au films are obtained by chemically dealloying AuAg solid solutions electrodeposited at different compositions in the range 30–50 at.% Au. Fig. 1a shows a nanoporous Au thin film (~1 μm) with an average filament diameter of 35 nm. Radiation damage in these materials mainly comes in the form of stacking fault tetrahedra (SFT) resulting from vacancy collapse. The interstitials annihilate at surfaces leaving no damage. Fig. 1b is a TEM micrograph of an irradiated sample showing evidence of SFT. Fig. 1c shows results from a computer simulation on melt-induced coarsening [32,33]. Molecular dynamics (MD) simulations have also provided insight on the lower limit of ligament dimensions during nanoporous synthesis [34].

The integration of computer simulations and experiments on these model nanoporous Au films, show that, for a given temperature, there exists a window in the parameter space of length scale and irradiation dose where such materials show radiation resistance (Fig. 1d). This window arises from the combined effect of two nanoscale characteristic length scales:

(i) the filament diameter below which the filament melts and breaks, together with compaction that increases with dose, while

(ii) the filament diameter above which it behaves as a bulk material and tends to accumulate damage.

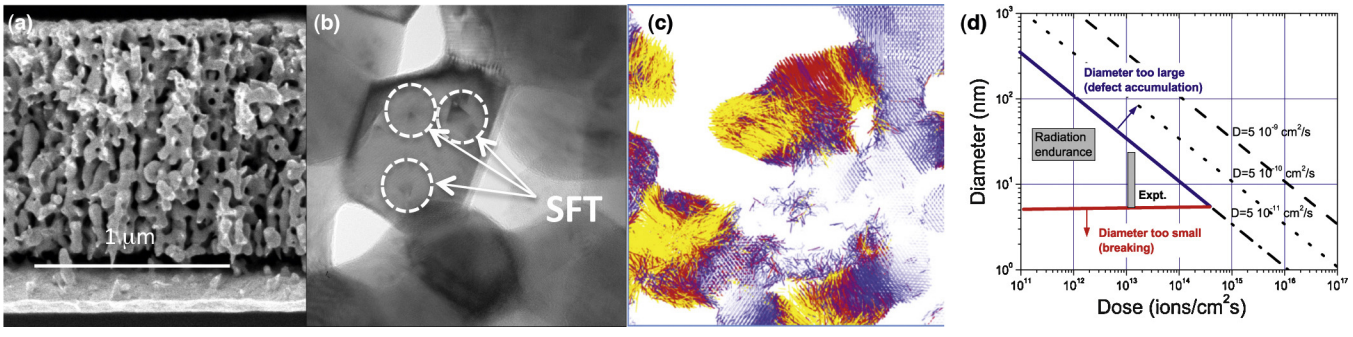

FIGURE 1

(a) SEM image of a 1 μm-thick Au nanofoam, (b) the main effect of irradiation on nanofoams is the formation of stacking fault tetrahedra (seen as triangular features within the filaments), as a result of the collapse of vacancy clusters, (c) radiation effects on thin filaments induce melting, as seen by this molecular dynamics simulation, in which colors indicate the magnitude of atomic displacement; yellow regions formed a continuous filament before irradiation and (d) window of radiation endurance in terms of filament diameter and radiation dose rate.

In between these dimensions is the window of optimal length scales where the defect migration to the filament surface is faster than the time between successive cascades, ensuring efficient defect recovery and radiation resistance.

The effect of irradiation on the mechanical behavior of nanoporous metals has also been investigated. The radiation-induced SFTs (Fig. 1b) can act as a source of dislocations inducing an unexpected irradiation softening behavior [35]. Further, the nanofoams exhibit a substantial tension/compression asymmetry in yield [36], for ligament sizes below ~10 nm. The large surface stresses in this case lead to residual compressive stresses in the ligament that favors yielding in compression. For ligament sizes below 1 nm, pore collapse under mechanical loading is reported causing an unexpected compaction under *tension* characterized by a decrease in the total volume of the sample of 15% [36].

Defect – grain boundary interactions in heavy ion irradiation

When experiments or models are used to understand the effect of grain boundaries on displacement damage caused by point defects, boundaries are typically either assumed to be generic in form [37] or static objects with fixed properties during irradiation [38]. Adopting this perspective, the interaction of defects with pristine boundaries has been calculated using atomistic simulations for a range of boundaries and materials, offering significant insight into how these interactions depend on boundary structure (see e.g., Ref. [39]).

Over the last 15 years or so, a growing body of evidence has pointed to the fact that reality departs significantly from these two ideals; that is, the structure matters and changes during irradiation. As first observed by Sugio *et al.* in 1998 [40], and later confirmed by a number of other groups (see Ref. [41] and references therein), MD simulations of collision cascades near grain boundaries reveal that grain boundaries interact strongly with the cascade, preferentially absorbing interstitials and leaving behind a defect structure within the grain interior that is vacancy rich. In many cases, so many interstitials are absorbed that in-cascade vacancy annihilation reduces and vacancy production increases beyond that expected without the grain boundary present. While the details do depend on the type of boundary considered [42], the effect is rather general, occurring in metals and ceramics, although curiously SiC seems to be an exception [41].

A corollary to this biased absorption is the fact that the grain boundaries, after interacting with the collision cascade, contain a significantly large concentration of defects, specifically interstitials. Recently, it has been discovered that these ''damaged'' boundaries interact with defects in a manner that is significantly different as compared to unirradiated boundaries. In particular, the thermodynamic interaction of defects with damaged boundaries tends to be both longer ranged and energetically much stronger than that with pristine boundaries [41,43]. The nature of these interactions depends on the concentration of defects at the boundaries, which itself is a consequence of radiation dose, flux, and time. This implies that the sink efficiency will also depend on irradiation conditions, as well as the grain boundary type, and boundaries should not be viewed as objects with properties that are constant with increasing dose. That is, as the defect content at the boundary changes, so will the rate of in-boundary annihilation and the interaction with nearby defects, both of which will affect the fluxes of defects to and from the boundary and thus its sink efficiency.

In particular, the excess interstitials at the boundaries interact strongly with nearby vacancies, leading to enhanced annihilation via ''interstitial emission'' mechanisms, Fig. 2 [43]. In such mechanisms, interstitials absorbed at the boundary annihilate vacancies that are several atomic planes away from the boundary via concerted events in which several atoms move during one thermally activated event, typically at much lower barriers than that for vacancy migration [43]. This annihilation mechanism leads to enhanced recovery, compared to if the vacancy had to migrate all the way to the boundary, and effectively extends the length-scale over which the defects and boundary interact. This mechanism must also be considered when determining sink efficiencies.

These results lead to new interpretations of the previously reported experimental results. For example, it has been observed that nanocrystalline Au accumulates damage faster than coarse-grain Au at low temperatures, but slower at high temperatures [44]. These results were interpreted as a consequence of reduced displacement threshold energy near the boundaries [45]. However,

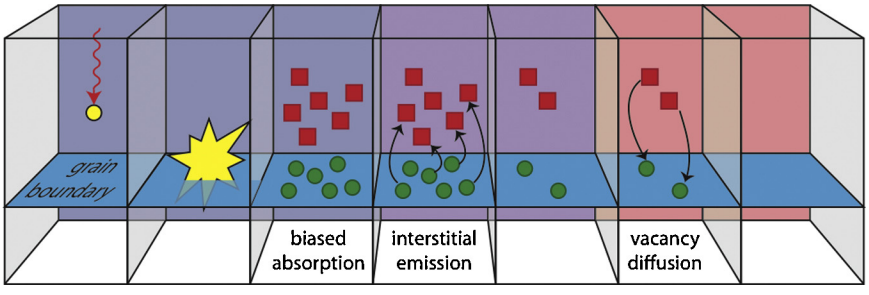

FIGURE 2

As collision cascades, caused by an incoming energetic particle, interact with a grain boundary, interstitials (green spheres) are preferentially absorbed by the boundary, leading to a state in which excess vacancies (red squares) are left in the grain interior. At low temperatures (the first three blue frames), nothing further can happen and the material accumulates damage faster than if the boundaries were not present. At intermediate temperatures (the second two purple frames), mechanisms with low activation energies such as interstitial emission can occur that annihilate some amount of the damage. At even higher temperatures (the last two red frames), vacancies become mobile and can diffuse directly to the boundary, maximizing the ability of grain boundaries to annihilate radiation damage.

these results can be explained by the biased absorption of interstitials. Further, when the low-temperature samples were annealed, faster recovery was observed in the nanocrystalline samples, even at temperatures where vacancy mobility is expected to be inconsequential [44]. This reversal in behavior suggests that a mechanism such as interstitial emission is active.

Another experimental result that is difficult to reconcile without invoking these effects is the observation that nanocrystalline $MgGa_2O_4$ is radiation tolerant [46], even at cryogenic temperatures where defect mobilities in the bulk are extremely small [47]. For there to be any significant annihilation rate, there must be some enhanced interaction between the defects and grain boundaries, which becomes significant when the boundaries contain excess defects. Indeed, in oxides, damaged boundaries can lead to electrostatic interactions that are longer ranged and stronger than the elastic interactions that dominate in metals [48].

Thus, to make quantitative predictions of radiation damage evolution in nanocrystalline materials, or even to obtain qualitative understanding of experimental results, it seems critical to consider that defect-boundary interactions vary with dose and thus time. Our future work will focus on quantifying these effects and determining the sensitivity of mesoscale response of the material to the details of these atomic scale mechanisms.

Predicting He-induced damage at solid-state interfaces

In contrast to the recovery of displacement damage discussed above, damage created through the introduction of impurities—either by implantation or transmutation—may be more difficult to avert. Unlike vacancies and interstitials, impurities have no ''opposite'' defect with which to recombine. Noble gasses such as helium (He) and xenon (Xe) are especially deleterious [49,50]. Because they are chemically inert, noble gasses are insoluble in most solids and precipitate out as bubbles, even if implanted in trace quantities.

A major breakthrough in understanding the effect of implanted noble gasses on the performance of structural materials was achieved in the mid-1980s with the discovery of the bubble-to-void transition [51,52]. This insight showed that nanometer-scale gas-filled bubbles are stable under irradiation so long as their volumes remain below a critical value. Above that value, they grow without bound into ''voids'' by capturing radiation-induced vacancies. Particle–matrix interfaces in dispersion-strengthened-metals have been shown to be efficient sites for trapping of nanoscale helium bubbles [10–12].

The bubble-to-void transition describes the fate of noble gas-filled cavities in crystals. In contrast, the effect of implanted noble gasses on interfaces between crystals remains less well understood. This is an important knowledge gap because it is He precipitation at homophase interfaces (grain boundaries)—not within crystalline grains—that is the likeliest cause of He-induced embrittlement in alloys used in nuclear energy applications [53,54]. Extending the lifetime of existing nuclear power plants beyond their initial design limits will require reliable assessments of He-induced degradation in these alloys, which, in turn, requires improved understanding of the effect of He on interfaces.

Using a combination of multiscale modeling [55,56] and several complementary experimental methods [57–61], we have shown that the nucleation and growth of He bubbles at interfaces involves an unexpected new kind of morphological transformation: the ''platelet-to-bubble'' transition. Much like the well-known bubble-to-void transition, platelet-to-bubble transitions are driven by a competition between three kinds of pressure acting on interfacial He-filled cavities: the mechanical pressure P_{He} of the trapped He gas, the osmotic pressure P_V due to the flux of radiation-induced vacancies within the crystal to the cavity, and the capillary pressure P_c arising from the surface energy of the cavity. P_{He} and P_V tend to expand the cavity while P_c tends to shrink it. If these three pressures balance, i.e.,

$$P_{He} + P_V = P_c,$$

then the cavity is in equilibrium: it neither expands nor contracts.

Inside crystalline metals, there is only one stable equilibrium configuration for He-filled cavities: an approximately spherical bubble of ~2 nm diameter. At certain interfaces, however, there is another stable state: platelet-shaped He-filled cavities. The origin of stable interfacial He platelets may be traced back to interface energy. Many interfaces have a characteristic location-dependent, internal structure. Associated with this structure is a non-uniform, location-dependent interface energy, such as that found at Cu–Nb interfaces and shown in Fig. 3. Some interfaces may contain regions with such high local energies that there is a thermodynamic driving force for He precipitates to wet these regions, much

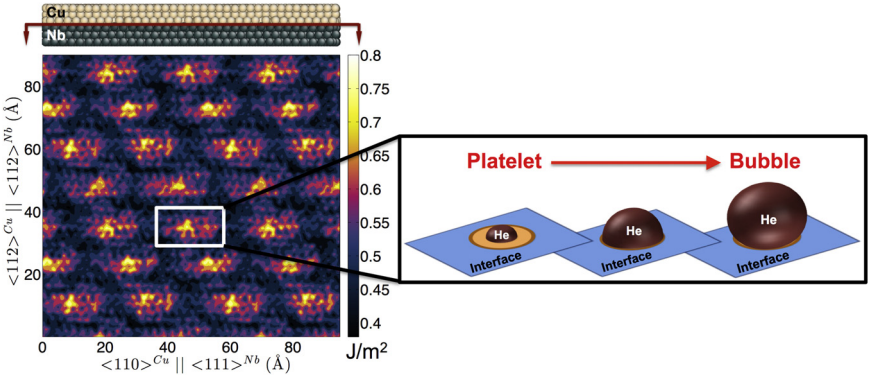

FIGURE 3

Left: location-dependent energy of Cu–Nb interfaces. The bright, high-energy regions are heliophilic. Right: a He platelet transforms into a bubble once it has grown to occupy the entire heliophilic patch on which it nucleated.

like water wets a glass pane. It is along such ''heliophilic'' interface regions that He platelets may grow.

Owing to their higher surface-to-volume ratios, platelets have higher capillary pressures than spherical bubbles. This higher capillary pressure balances the mechanical and osmotic pressures that tend to expand the platelet, stabilizing it against growth into a spherical bubble. However, if a platelet should grow larger than the ''heliophilic'' interface region on which it nucleated and expanded into surrounding lower-energy, ''heliophobic'' regions, the capillary pressure drops precipitously. This drop may de-stabilize the He platelet, causing it to expand rapidly into a He bubble, as illustrated in Fig. 3.

These insights suggest a pathway toward understanding and predicting the behavior of He on any interface. Using atomistic modeling, the location-dependent energy of the interface may be determined and used to calculate wetting coefficients for different parts of the interface [56]. The distribution of wetting and non-wetting regions defines the maximum size and areal density of interfacial He platelets. It may also be used to determine the number of He atoms that can be stably stored in interfacial platelets without forming bubbles. Such predictions are invaluable in calculating the expected lifetime of polycrystalline engineering materials when exposed to long-term He implantation.

Processing of bulk nanocomposites with stable interfaces

Although the concept of enhanced defect recovery or stable helium storage has been demonstrated in the above examples, utilizing such advanced materials commercially relies on the ability to manufacture bulk nanocomposites that contain interfaces that are stable under irradiation at elevated temperatures.

Nanostructuring via severe plastic deformation (SPD) has become a popular method for fabricating nanomaterials in structural size scales [62]. This grain-refining technique is a top-down process that can transform a traditional coarse-grained metal into a nanocrystalline metal without changing the original dimensions of the sample [62]. Experiments have shown that the resulting increases in the fraction of grain boundaries can lead to several-fold increases in strength [63–65]. Impressive though this result may be, the grain boundaries created by mechanical processing are disordered (high energy, tangled networks of defects) [62] and unstable at high temperatures [66]. Consequently, they do not retain their outstanding strength at elevated temperature, although suppression of grain growth through solute segregation to the boundary may impart thermal stability [67].

In an attempt to overcome this problem, we applied an SPD process to a composite of two dissimilar metals with the aim of creating a strong and thermally stable nanostructured metal. Compared to grain boundaries, bimetal interfaces between two metals with minimal solid solubility would be much more stable under elevated temperatures. Moreover, when spaced several nanometers apart, they can act as effective barriers to dislocation motion and sinks for radiation-induced point defects and traps for helium as discussed in the earlier sections.

Specifically we fabricated Cu–Nb nanocomposite materials in bulk form (>cm^3) with a processing technique called accumulative roll bonding (ARB) [68,69]. To minimize the introduction of oxides to the interfaces, a specially designed ARB process was used [70]. Our ARB process delivers two-phase (Cu–Nb) samples with controllable layer thicknesses from submicron to the nanoscale (down to 10 nm) [70,71]. Fig. 4a shows the typical nanolayered microstructure with planar Cu–Nb interfaces spaced approximately 20 nm apart [71]. As demonstrated in Fig. 5a, the size of the sample (cm^3) from which this was taken was several orders of magnitude larger than the layer thickness. The ARB process combines an unprecedented level of control of nm-scale structure with the ability to fabricate large volumes of material.

The crystallographic textures of these nanocomposites, measured by neutron diffraction [68], were unusually sharp and significantly different from the rolling textures of monolithic fcc or bcc metals. The saturation in texture at approximately 10 nm layer thickness indicated a preferred stable interface that was confirmed by high-resolution transmission electron microscopy (TEM) [72]. It was found that the Cu layer exhibited deformation twinning, starting at a layer thickness (h) of 100 nm and increasing in frequency as the layers were further refined to $h = 10$ nm [68,73]. Remarkably, in spite of severe plastic deformation, the interfaces in the $h = 10$ nm material were sharp and exhibited a periodic array of facets (Fig. 4b). The crystallography of the interface shown in Fig. 4b is $\{5\,5\,1\}\langle 1\,1\,0\rangle$Cu||$\{1\,1\,2\}\langle 1\,1\,1\rangle$Nb (referred to as the '*Z*-interface'), which does not correspond to that of an

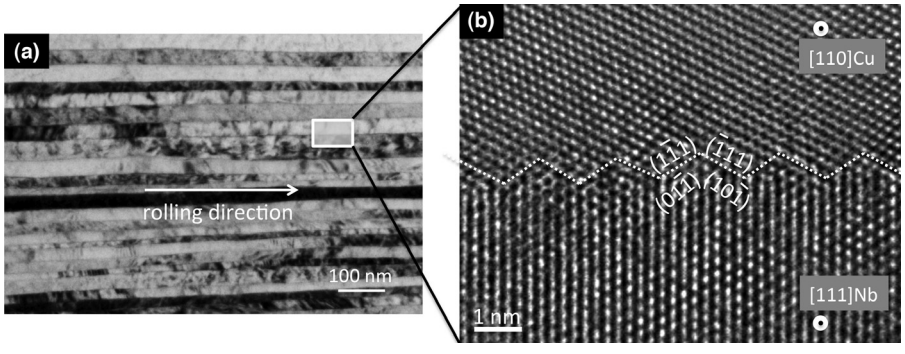

FIGURE 4

(a) TEM micrograph of the Cu–Nb layered composite fabricated by severe plastic deformation process called accumulative roll bonding. The Cu–Nb interfaces are spaced 20 nm apart and (b) high resolution TEM micrograph showing the regular atomic structure of the predominant Cu–Nb interface that prevails over most of the nanocomposite (layer thickness 10 nm).

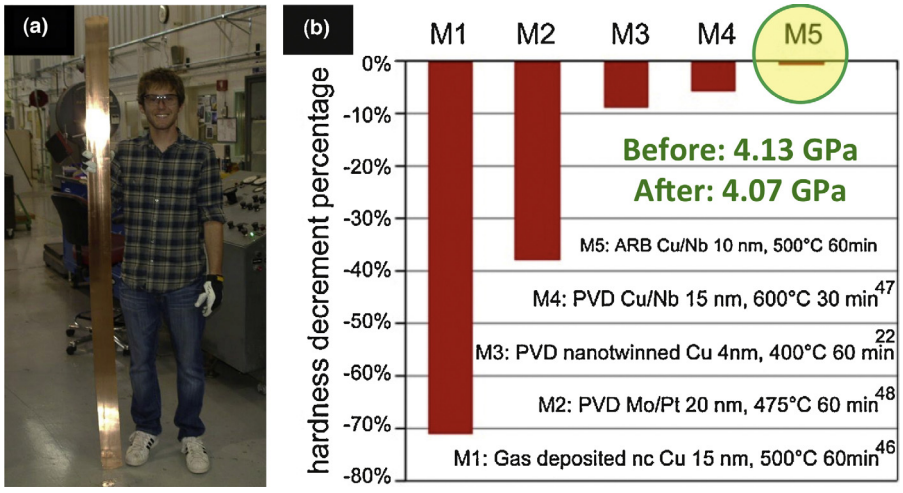

FIGURE 5

(a) Student, Tom Nizolek, holding ~4 mm thick workpiece of a Cu–Nb nanocomposite fabricated by ARB processing. This synthesis pathway has the advantage of producing bulk quantities of nanocomposite with a controllable bimetal interfacial character, (b) hardness decrement of the ARB Cu–Nb material (marked as material "M5") as compared to other nanomaterials after annealing [76–79]. Note that the ARB Cu–Nb material maintains its hardness after annealing, exhibiting enhanced thermal stability over other nanomaterials.

interface that would arise from thermodynamic processes (such as eutectic solidification). Atomic-scale modeling was used to predict the relaxed structure of this preferred Cu–Nb *Z*-interface. The agreement in faceted structure with the actual interface in Fig. 4b is noteworthy [72]. The persistence of the interface crystallography with low-energy facets suggests its stability during rolling to large plastic strains.

To gain a detailed understanding of the crystallographic stability of the interfaces during ARB, we examined several interfaces varying in interface character using atomistic modeling [74] and crystal plasticity [75]. Bicrystal simulations show that the interface that forms after twinning $\{5\,5\,2\}\langle 1\,1\,0\rangle$Cu$||\{1\,1\,2\}\langle 1\,1\,1\rangle$Nb is unstable under the rolling process. Via dislocation slip, the interface transforms to a more stable configuration between the *Z* interface and $\{1\,1\,0\}\langle 0\,0\,1\rangle$Cu$||\{1\,1\,2\}\langle 1\,1\,1\rangle$Nb interface. These two interfaces are misoriented by only 8°. MD simulations reveal that within this 8° narrow range, the *Z*-interface corresponds to an energy well. Therefore, the *Z*-interface that emerges is stable in crystallographic character and formation energy.

The stability of the low-energy faceted interface produced by ARB was examined by annealing at elevated temperatures. After annealing at nearly half the homologous melting temperature of Cu, the hardness of the 10 nm nanocomposite decreased only 1% (from 4.13 ± 0.4 GPa to 4.07 ± 0.2 GPa) [72]. Fig. 5b compares the hardness retention of these composites with other nanostructured Cu-based composites [76–79]. Notably the ARB h = 10 nm material experienced the least reduction in strength. High-resolution TEM showed the preservation of the layered morphology and the low-energy atomic structure after annealing.

Interestingly, this outstanding thermal stability equals that of Cu–Nb nanolayered physical vapor deposition (PVD) foils, which are known to have epitaxially oriented layers with interfaces of minimum energy [76,80]. However, unlike the ARB sheet material, the PVD foils cannot be fabricated in abundant quantities for structural applications. Currently, the ARB method is being applied to other material systems, such as Zr–Nb [81].

Recent experiments have shown that the ion irradiation responses of ARB and PVD Cu–Nb interfaces are similar [82]. These studies show that interfaces in nanocomposites that are mechanically stable under severe plastic deformation are also stable under ion irradiation and serve to provide radiation damage tolerance in bulk nanocomposites.

Conclusions

An integrated modeling and experimental approach on carefully selected model systems, often involving epitaxially oriented layers in thin film geometry, is shown to be crucial in elucidating the key unit mechanisms of the interactions between interfaces and radiation-induced point defects and impurities such as helium. We have also demonstrated that such mechanisms can be realized in bulk nanocomposites where severe plastic deformation can drive the formation of stable, low-energy interfaces. In future, such studies can guide the development of bulk nanocomposites in shapes, sizes and tailored response as required for the next-generation automotive, aerospace and nuclear reactor applications.

Acknowledgements

This work was supported by the U.S. Department of Energy, Office of Science, Office of Basic Energy Sciences (DOE/BES) under Award No. 2008LANL1026 through the Center for Materials at Irradiation and Mechanical Extremes, an Energy Frontier Research Center. Access to the Center for Integrated Nanotechnologies, a DOE/BES sponsored user facility is acknowledged. Work on nanoporous metal synthesis was supported by LANL-LDRD program. Authors acknowledge discussions with R.G. Hoagland, J.P. Hirth, W.D. Nix, G.R. Odette, M. Nastasi, M.I. Baskes, A. Sutton, F. Williame, A.D. Rollett, R.S. Averback, P. Bellon, and T.M. Pollock.

References

[1] Basic Research Needs Workshop Reports, Advanced Nuclear Energy Systems, and Materials under Extreme Environments, DOE, Office of Basic Energy Sciences, http://science.energy.gov/bes/news-and-resources/reports/basic-research-needs/.

[2] S.J. Zinkle, G.S. Was, Acta Mater. 61 (2013) 735–758.
[3] S.J. Zinkle, J.T. Busby, Mater. Today 12 (2009) 12–19.
[4] A. Misra, L. Thilly, MRS Bull. 35 (12 (December)) (2010) 965–976.
[5] B.N. Singh, Philos. Mag. 29 (1974) 25–42.
[6] Y. Matsukawa, S.J. Zinkle, Science 318 (2007) 959–962.
[7] S.J. Zinkle, K. Farrell, J. Nucl. Mater. 168 (1989) 262.
[8] P.A. Thorsen, J.B. Bilde-Sorensen, B.N. Singh, Scr. Mater. 51 (2004) 557.
[9] R.B. Adamson, W.L. Bell, P.C. Kelly, J. Nucl. Mater. 92 (1980) 149.
[10] K. Farrell, et al. Radiat. Eff. Defects Solids 78 (1983) 277–295.
[11] G.R. Odette, M.J. Alinger, B.D. Wirth, Annu. Rev. Mater. Res. 38 (2008) 471.
[12] G.R. Odette, D.T. Hoelzer, JOM 62 (2010) 84–92.
[13] L. Barnard, et al. Acta Mater. 60 (2012) 935–947.
[14] D. Bhattacharyya, et al. Philos. Mag. 92 (2012) 2089–2107.
[15] E.A. Marquis, et al. Mater. Today 12 (2009) 30–37.
[16] Z. Oksiuta, et al. J. Mater. Sci. 48 (2013) 4620–4625.
[17] A. Certain, et al. J. Nucl. Mater. 434 (2013) 311–321.
[18] M.-L. Lescoat, et al. J. Nucl. Mater. 428 (2012) 176–182.
[19] M.C. Brandes, et al. Acta Mater. 60 (2012) 1827–1839.
[20] A. Hirata, et al. Nat. Mater. 10 (2011) 922–926.
[21] M.J. Demkowicz, A. Misra, A. Caro, Curr. Opin. Solid State Mater. Sci. 16 (June) (2012) 101–108.
[22] M.J. Demkowicz, R.G. Hoagland, J.P. Hirth, Phys. Rev. Lett. 100 (2008) 136102–136105.
[23] M. Samaras, et al. Phys. Rev. Lett. 88 (2002) 125505–125508.
[24] A. Misra, et al. JOM 59 (2007) 62–65.
[25] S.J. Zheng, et al. Nat. Commun. 4 (April) (2013) 1696.
[26] N.B. Heubeck, Nuclear fuel elements made from nanophase materials. US Patent 5,805,657 (1998).
[27] K. Forsberg, A.R. Massih, J. Nucl. Mater. 135 (1985) 140.
[28] L.S. Novikov, et al. J. Surf. Invest. X-ray Synchrotron Neutron Tech. 3 (2009) 199–214.
[29] M.E. Palumbo, Astron. Astrophys. 453 (2006) 903.
[30] U. Raut, et al. J. Chem. Phys. 126 (2007) 244511.
[31] J.F. Rodriguez-Nieva, et al. Astrophys. J. Lett. 743 (2011) L5.
[32] E.M. Bringa, et al. Nano Lett. 12 (2012) 3351–3355.
[33] E.G. Fu, et al. Appl. Phys. Lett. 101 (2012) 191607.
[34] K. Kolluri, M.J. Demkowicz, Acta Mater. 59 (2011) 7645–7653.
[35] L. Zepeda-Ruiz, J.A. Caro, private communication.
[36] D. Farkas, et al. Acta Mater. 61 (2013) 3249–3256.
[37] L.K. Mansur, J. Nucl. Mater. 216 (1994) 97.
[38] S. Watanabe, et al. J. Phys. IV France 10 (2000) Pr6-173.
[39] M.A. Tschopp, et al. Phys. Rev. B 85 (2012) 064108.
[40] K. Sugio, Y. Shimomura, T.D. de la Rubia, J. Phys. Soc. Jpn. 67 (1998) 882.
[41] X.M. Bai, B.P. Uberuaga, JOM 65 (2013) 360.
[42] X.M. Bai, et al. Phys. Rev. B 85 (2012) 214103.
[43] X.M. Bai, et al. Science 327 (2010) 1631.
[44] Y. Chimi, et al. J. Nucl. Mater. 297 (2001) 355.
[45] Y. Chimi, et al. Nucl. Instrum. Methods B 245 (2006) 171.
[46] T.D. Shen, et al. Appl. Phys. Lett. 90 (2007) 263115.
[47] B.P. Uberuaga, et al. Phys. Rev. B 75 (2007) 104116.
[48] B.P. Uberuaga, et al. J. Phys.: Condens. Matter 25 (2013) 355001.
[49] H. Trinkaus, B.N. Singh, J. Nucl. Mater. 323 (2003) 229–242.
[50] X.Y. Liu, et al. Appl. Phys. Lett. 98 (2011) 151902.
[51] L.K. Mansur, W.A. Coghlan, J. Nucl. Mater. 119 (1983) 1–25.
[52] R.E. Stoller, G.R. Odette, J. Nucl. Mater. 131 (1985) 118–125.
[53] H. Schroeder, W. Kesternich, H. Ullmaier, Nucl. Eng. Des. 2 (1985) 65–95.
[54] D.N. Braski, H. Schroeder, H. Ullmaier, J. Nucl. Mater. 83 (1979) 265–277.
[55] A. Kashinath, M.J. Demkowicz, Model. Simul. Mater. Sci. Eng. 19 (2011) 035007.
[56] A. Kashinath, A. Misra, M.J. Demkowicz, Phys. Rev. Lett. 110 (2013) 104116.
[57] M.J. Demkowicz, et al. Appl. Phys. Lett. 97 (2010) 161903.
[58] E.G. Fu, et al. J. Nucl. Mater. 407 (2010) 178–188.
[59] N. Li, et al. Philos. Mag. Lett. 91 (2010) 19–29.
[60] A. Kashinath, et al. J. Appl. Phys. 114 (2013) 043505.
[61] J. Hetherly, et al. Scr. Mater. 66 (2012) 17–20.
[62] R.Z. Valiev, T.G. Langdon, Prog. Mater. Sci. 51 (2006) 881–981.
[63] R.Z. Valiev, et al. J. Mater. Res. 17 (2002) 5–8.
[64] G.G. Yapici, et al. Acta Mater. 55 (2007) 4603–4613.
[65] Y.T. Zhu, et al. MRS Bull. 35 (2010) 977–981.
[66] J.R. Weertman, Science 337 (2012) 921–922.
[67] T. Chookajorn, H.A. Murdoch, C. Schuh, Science 337 (2012) 951–954.
[68] J.S. Carpenter, et al. Acta Mater. 60 (2012) 1576–1586.
[69] S.-B. Lee, et al. Acta Mater. 60 (2012) 1747–1761.
[70] I.J. Beyerlein, et al. JOM 64 (10) (2012) 1192–1207.
[71] S.J. Zheng, et al. Acta Mater. 60 (2012) 5858–5866.
[72] S.J. Zheng, et al. Nat. Commun. 4 (2013) 1696.
[73] I.J. Beyerlein, et al. Mater. Res. Lett. 1 (2013) 85–89.
[74] K. Kang, et al. J. Appl. Phys. 112 (2012) 073501.
[75] J.R. Mayeur, et al. Int. J. Plast. 48 (2013) 72–91.
[76] A. Misra, R.G. Hoagland, J. Mater. Res. 20 (2005) 2046–2054.
[77] O. Anderoglu, et al. Appl. Phys. 103 (2008) 094322.
[78] M. Kobiyama, T. Inami, S. Okuda, Scr. Mater. 44 (2001) 1547–1551.
[79] A. Bellou, L. Scudiero, D.F. Bahr, J. Mater. Sci. 45 (2010) 354–362.
[80] A. Misra, R.G. Hoagland, H. Kung, Philos. Mag. 84 (2004) 1021–1028.
[81] M. Knezevic, et al. Mater. Res. Lett. 1 (2013) 133–140.
[82] W. Han, et al. Advanced Materials (2013), http://dx.doi.org/10.1002/adma.201303400 (in press).